Bcl-x$_L$ regulates metabolic efficiency of neurons through interaction with the mitochondrial F$_1$F$_O$ ATP synthase

Kambiz N. Alavian[1,*], **Hongmei Li**[1,*], **Leon Collis**[2,*], **Laura Bonanni**[3], **Lu Zeng**[1], **Silvio Sacchetti**[1,4], **Emma Lazrove**[1], **Panah Nabili**[1], **Benjamin Flaherty**[1], **Morven Graham**[5], **Yingbei Chen**[6], **Shanta Messerli**[2], **Maria A. Mariggio**[4], **Christoph Rahner**[5], **Ewan McNay**[7], **Gordon Shore**[8], **Peter J. S. Smith**[2,10], **J. Marie Hardwick**[6,9], and **Elizabeth A. Jonas**[1]

[1]Dept. Internal Medicine, Yale University, New Haven, CT, USA [2]Biocurrents Research Center, Marine Biological Laboratory, Woods Hole, MA, USA [3]Dept. Oncology and Neuroscience and Aging Research Center, University G.D'Annunzio of Chieti-Pescara, Italy [4]Dept. Biochemistry, Physiology and Pathology of Muscle, Basic and Applied Medical Sciences Università G.D'Annunzio of Chieti-Pescara, Italy [5]Dept. Cell Biology, Yale University, New Haven, CT, USA [6]Dept. Pharmacology and Molecular Sciences, Johns Hopkins, Baltimore, MD, USA [7]Behavioural Neuroscience and Center for Neuroscience Research, University at Albany, NY, USA [8]Gemin X Pharmaceuticals, Montréal, QC, Canada [9]Molecular Microbiology and Immunology, Johns Hopkins, Baltimore, MD, USA [10]Institute for Life Sciences, University of Southampton, England

Abstract

Anti-apoptotic Bcl2 family proteins such as Bcl-x$_L$ protect cells from death by sequestering apoptotic molecules, but also contribute to normal neuronal function. We find in hippocampal neurons that Bcl-x$_L$ enhances the efficiency of energy metabolism. Our evidence suggests that Bcl-x$_L$ interacts directly with the beta subunit of the F$_1$F$_O$ ATP synthase, decreasing an ion leak within the F$_1$F$_O$ ATPase complex and thereby increasing net transport of H$^+$ by F$_1$F$_O$ during F$_1$F$_O$ ATPase activity. By patch clamping submitochondrial vesicles enriched in F$_1$F$_O$ ATP synthase complexes, we find that, in the presence of ATP, pharmacological or genetic inhibition of Bcl-x$_L$ increases the membrane leak conductance. In addition, recombinant Bcl-x$_L$ protein directly increases ATPase activity of purified synthase complexes, while inhibition of endogenous Bcl-x$_L$ decreases F$_1$F$_O$ enzymatic activity. Our findings suggest that increased mitochondrial efficiency contributes to the enhanced synaptic efficacy found in Bcl-x$_L$ expressing neurons.

*These authors contributed equally to the work.

Introduction

Bcl2 family proteins regulate programmed cell death[1–3]. In brain, neurons are eliminated during development, and after insults such as ischemia, infection or trauma[1–3]. The mechanisms by which anti-apoptotic proteins such as Bcl2 and Bcl-x_L prevent death are incompletely understood. Bcl-x_L sequesters pro-apoptotic members of the Bcl2 family and BH3-only proteins[4–6]. Additionally, Bcl-x_L enhances metabolite exchange between mitochondria and the cytosol through interaction with VDAC, helping prevent release of death-promoting factors[7].

Bcl-x_L is often highly expressed in cancer cells resistant to cell death, but also functions in neuronal plasticity. Bcl-x_L is the predominant anti-apoptotic protein in adult brain[8]. Over-expression of Bcl-x_L increases the number and size of synapses, localizes mitochondria to presynaptic sites[9] and increases mitochondrial biomass[10].

As synapses develop and grow, the formation of a larger reserve of neurotransmitter-containing vesicles contributes to more frequent or prolonged synaptic events[11]. The function of these larger pools of synaptic vesicles depends on metabolism and position of mitochondria at the synapse[12]. Certain mitochondrial-interacting proteins such as Drp1 and Bcl-x_L participate in synaptic strengthening or vesicle recovery after high frequency firing[3, 12–14]. Since high metabolic demand occurs during synaptic strengthening, a possible action of Bcl-x_L is to increase the release or production of mitochondrial metabolites during synaptic plasticity.

We have now found that neurons over-expressing Bcl-x_L have higher ATP levels, and cells in which endogenous Bcl-x_L is depleted or inhibited have lower ATP levels. Despite the increase in ATP, neurons over-expressing Bcl-x_L use less oxygen, while Bcl-x_L depletion increases oxygen uptake. In addition to its outer membrane localization, we find Bcl-x_L in the mitochondrial matrix by immuno-EM. Bcl-x_L co-immunoprecipitates with the beta subunit of F_1F_O ATP synthase and binds to purified recombinant beta subunit of the F_1 ATP synthase. Exogenously applied Bcl-x_L increases F_1F_O ATPase activity, while Bcl-x_L inhibition decreases enzymatic rate. Bcl-x_L deficiency reduces the capacity of F_1F_O ATPase-containing submitochondrial vesicles to sequester H^+ ions, suggesting that Bcl-x_L depletion causes protons to leak upon activation of the enzyme. By patch clamping F_1F_O ATPase-containing vesicles exposed to ATP, we record an increased leak conductance when Bcl-x_L is inhibited or depleted. We therefore suggest a model whereby Bcl-x_L increases the efficiency of ATP synthesis by decreasing a proton leak within the F_1F_O ATPase, thus improving neuronal metabolism.

RESULTS

ATP levels are elevated in Bcl-x_L over-expressing neurons and decreased in Bcl-x_L-depleted neurons

To determine the effect of Bcl-x_L on ATP levels in neurons, luminescence of firefly luciferin;luciferase was measured in cultured hippocampal neurons expressing lentivirus constructs for GFP- Bcl-x_L or control GFP[15]. ATP levels in GFP-Bcl-x_L expressing cultures

were approximately twice that of non-transduced or GFP-expressing controls (Fig. 1a, Fig. S1a). Knockdown of Bcl-x_L with shRNA-carrying lentivirus but not with scrambled control virus decreased ATP levels (Fig. 1b,c), although cell death was not significantly different at the time of the study (Fig. S1b). As a further test of the effect of endogenous Bcl-x_L on ATP levels, Bcl-x_L activity was pharmacologically inhibited by ABT-737, a mimetic of BH3-only proteins that binds to Bcl-x_L[14, 16]. ATP levels were decreased in cultures exposed to ABT-737 (Fig. 1d).

Measurements of luminescence in lysed cells cannot accurately indicate ongoing levels of ATP production in live neurons. Therefore, to measure ATP levels in live neurons (excluding glia), neurons were engineered to express luciferase by lentiviral transduction (Fig. 1d). Application of luciferin led to an immediate rise in luminescence (Fig. 1e calibrated to known concentrations of ATP). Such calibrated light levels were significantly higher in GFP-Bcl-x_L expressing neurons compared to Mito-GFP controls (Fig. 1f).

Elevated ATP levels in the Bcl-x_L over-expressing cultures could be explained by an increase in aeorobic glycolysis. To determine if glycolysis is increased by Bcl-x_L, lactate production was assessed by measuring lactate levels in the medium. Lactate level was significantly higher in controls compared to the Bcl-x_L-expressing neurons, suggesting that Bcl-x_L cells perform less glycolysis than controls (Fig. 1g). To further test the use of mitochondrial metabolism, cell viability was measured in a medium containing only mitochondrial substrates (Supple Fig. 1c). GFP- Bcl-x_L-over-expressing cells had improved survival compared to controls, suggesting enhanced mitochondrial competence.

Bcl-x_L decreases mitochondrial oxygen uptake

Previous work described increased mitochondrial biomass in neurons over-expressing Bcl-x_L[10] (also see Fig. S2). If increased mitochondrial biomass were solely responsible for increased ATP levels, then Bcl-x_L-expressing cells would be expected to have increased oxygen uptake. To examine this, oxygen uptake was measured in single neurons in culture using a sensitive self-referencing oxygen electrode[17] (Fig. 2a and Fig. S3a,b). Contrary to expectation, oxygen flux of Bcl-x_L over-expressing neurons was lower than that of mito-GFP-transfected neurons (Fig. 2b), suggesting that Bcl-x_L over-expressing neurons couple ATP production more efficiently to oxygen uptake. Endogenous Bcl-x_L has a similar effect because shRNA-mediated depletion (Fig. 2c,d) or pharmacological inhibition of Bcl-x_L (Fig. 2e) increased oxygen flux by neurons. These data suggest that depletion or inhibition of Bcl-x_L uncouples ATP production from oxygen uptake[18–20].

The higher ATP levels and lower oxygen uptake of Bcl-x_L-over-expressing neurons could, in theory, result from a quiescent state where ATP accumulates due to reduced electrical and synaptic activity. This is unlikely because Bcl-x_L over-expressing neurons have larger synapses and more spontaneous activity than controls[9, 10]. Therefore, we tested if Bcl-x_L over-expressing neurons have a greater but underutilized energetic capacity. Bcl-x_L over-expressing neurons increased oxygen flux by approximately 90% over basal when cells were depolarized with high potassium (High K), a treatment known to stimulate neuronal electrical and synaptic activity[21, 22] (example shown in Fig. 2f) whereas Mito-GFP-expressing controls enhanced flux by only 50%.

During oxidative phosphorylation, protons pumped out of the mitochondrial matrix re-enter the matrix by 1) flux of H^+ across the inner mitochondrial membrane at the ATP synthase (productive flux) and 2) a H^+ leak (non-productive)[23]. A decrease in the non-productive leak increases the efficiency of ATP production. To determine if Bcl-x_L-over-expressing neurons have a different degree of non-productive leak across the inner membrane than controls during maximal activity, High K was rapidly washed out of the bath and oxygen uptake was measured in oligomycin, which inhibits H^+ flux associated with ATP production, but does not inhibit H^+ flux associated with the non-productive leak[24]. GFP-Bcl-x_L cells had a higher ratio of productive oxygen flux to total oxygen flux compared to mito-GFP expressing controls, indicating that they use a higher percentage of the overall peak oxygen flux to make ATP (Fig. 2g).

Bcl-x_L enhances ATP synthesis during neuronal activity

Neurons could regulate metabolism during periods of increased activity. To study the role of Bcl-x_L in such enhanced energy production, we stimulated neurons with high K and measured cytosolic ATP levels 5min. after stimulation had ceased. Remarkably, levels of ATP were increased, suggesting a requirement for enhanced energy production that outlasted the period of stimulation. Such increase in ATP levels was completely prevented by pre-exposure for 5min. of the neurons to the Bcl-x_L inhibitor ABT-737, suggesting that Bcl-x_L was specifically required for the stimulation-induced metabolic change (Fig. 2h).

Bcl-x_L is localized to the mitochondrial inner membrane

Most of the previous studies have defined a role for Bcl-x_L in mitochondrial outer membranes as a regulator of cell death or in releasing metabolites from mitochondria[25–29], but a few studies have also suggested a localization of the related anti-apoptotic proteins Bcl2[30, 31] and Bcl-x_L (Hardwick Lab, unpublished data) to the inner membrane. To confirm and extend these findings, we checked for mitochondrial localization of Bcl-x_L in the Bcl-x_L over-expressing hippocampal neurons and in control rodent brain, immuno-electron microscopy (immuno-EM) was performed. Bcl-x_L was localized to the outer membrane and inner membrane or matrix of mitochondria of GFP- Bcl-x_L expressing neurons (Fig. 3a) and native brain mitochondria (Fig. 3b). Furthermore, Bcl-x_L (large gold beads) was co-localized at the inner membrane cristae with a known inner membrane cristae protein Manganese Super Oxide Dismutase (MnSOD; small gold beads, Fig. 3b)[32–34]. Overall, Bcl-x_L was localized about equally to inner membrane or matrix and to outer membrane (Fig. 3c). Previous reports localize the anti-apoptotic protein Bcl2 to the mitochondrial inner membrane[30, 31, 35] or Bcl-x_L to the same compartment as mitochondrial ATP synthase (Hardwick lab, unpublished data). To determine if Bcl-x_L was indeed localized within this compartment, submitochondrial vesicles of the inner membrane that are enriched in F_1F_O ATP synthase protein complexes (SMVs) and lack an outer membrane were prepared from whole rat brain[36, 37]. Bcl-x_L was present by immunoblot in this purified sample (Fig. S4). To further localize Bcl-x_L within the inner membrane, the protein was co-immunoprecipitated with the ATP synthase complex beta-subunit using either a specific antibody against Bcl-x_L or a specific antibody against ATP synthase beta-subunit (Fig. 3d). To determine the exact binding site of Bcl-x_L, recombinant FLAG- and myc-tagged proteins of the ATP synthase subunits alpha, beta, c, d, delta, epsilon, gamma and OSCP were

immunoprecipitated from mammalian 293T cells using beads conjugated to anti-FLAG antibody. Endogenous Bcl-x_L co-immunoprecipitated only with alpha and beta subunits (Fig. 3e). The interaction with beta-subunit was blocked by the specific Bcl-x_L inhibitor ABT-737, suggesting that the beta-subunit binds to Bcl-x_L within the ABT-737 binding pocket (Fig. 3f).

Recombinant Bcl-x_L protein enhances enzymatic rate of the F_1F_O ATPase

To determine if Bcl-x_L affects enzymatic activity of F_1F_O ATPase, the rate of ATP hydrolysis was quantified in SMVs[36, 37]. Vesicles were treated with triton-x to isolate the F_1F_O ATPase enzyme complex from the membrane. Activity of the F_1F_O ATPase was prevented by the ATP synthase inhibitor oligomycin, confirming the specificity of the reaction to the F_1F_O ATPase complex (Fig. 4a). Addition of recombinant Bcl-x_L protein increased the rate of ATP hydrolysis (Fig. 4a) over that measured after addition of control protein (bovine serum albumin (BSA), suggesting that interaction of Bcl-x_L protein with the F_1F_O ATPase increases enzymatic rate. Bcl-x_L protein itself had no effect on luciferase activity in the absence of SMVs (1.000 ± 0.008 vs. 0.994 ± 0.006 without and with Bcl-x_L, normalized to controls, N=5 wells each). In addition, the N terminus of Bcl-x_L was not required, since recombinant Bcl-x_L protein lacking the N-terminus (DeltaN Bcl-x_L) also increased the rate of ATP hydrolysis (Fig. S5a). To test if endogenous Bcl-x_L contributed to enzymatic rate, F_1F_O ATPase was exposed to ABT-737. ABT-737 decreased the rate of ATP hydrolysis (Fig. 4b), while DMSO carrier had no effect (Fig. S5b; N=3).

The enzymatic activity of the F_1F_O ATPase was also measured in an ATP-regenerating assay where ATP concentration cannot be rate-limiting. Recombinant Bcl-x_L protein significantly enhanced the enzymatic rate of the F_1F_O ATPase; inactive Bcl-x_L protein had no effect (Fig. 4c); ABT-737 and another small molecule inhibitor of Bcl-x_L, Obatoclax[38] significantly decreased enzymatic rate. The effect of Bcl-x_L was mimicked by application of a recombinant truncated Bcl-x_L protein lacking the membrane-targeting region (Delta-TM Bcl-x_L), indicating that specific membrane targeting is not necessary for this effect (Fig. 4c). These studies suggest that endogenous or exogenously applied Bcl-x_L enhance enzymatic rate of the F_1F_O ATPase, and that the N and C termini are not required for these effects. Furthermore, there was no change in the rate of ATP hydrolysis upon exposure to membrane ionophores, nystatin or FCCP, (N=3 samples each, Fig. S5c), suggesting that the channel-producing function of Bcl-x_L is not responsible for the enhanced enzymatic rate of F_1F_O ATPase.

Bcl-x_L inhibition attenuates H^+ sequestration into submitochondrial vesicles during F_1F_O ATPase activity

The oxygen flux studies had revealed an oligomycin-insensitive, Bcl-x_L-sensitive leak of H^+ that could contribute to inefficiency of ATP production. To measure H^+ leak during F_1F_O ATPase enzymatic activity, we measured movement of H^+ ions into the SMVs in response to ATP hydrolysis. After addition of ATP to the SMVs, ATPase activity results in a decrease in H^+ concentration in the bath surrounding the vesicles[39] measured by a decrease in fluorescence of the SMV-excluded H^+ indicator, ACMA[39] (Fig. 5a). Addition of ATP to the control buffer in the absence of SMVs failed to change ACMA fluorescence ($99.2 \pm 1\%$

control, N=6) whereas addition of ATP to SMVs resulted in a marked decrease in fluorescence (Fig. 5b,c). Attenuation of the maximum response to ATP occurred either upon inhibition of H^+ ion import through the F_O pump (oligomycin), or by leakage of H^+ out of the SMVs (FCCP). Attenuation also occurred in the presence of two different small molecule Bcl-x_L inhibitors, ABT-737[16] or Obatoclax[38] (Fig. 5b,c), consistent with the hypothesis that inhibition of endogenous Bcl-x_L decreases enzymatic rate or induces a H^+ leak within the SMV membrane.

Patch clamp recordings of submitochondrial vesicles reveal a Bcl-x-L-sensitive membrane leak

To more directly measure leak conductance, we developed a method to patch clamp the SMVs isolated from native rat brain. This method was based on our previous published methods in which we had patch-clamped similarly sized organelles (500–1000nm in diameter) either within living presynaptic terminals or isolated from brain, using pipettes with diameters of ~180nm[3, 40, 41]. In intracellular solution lacking ATP in both the bath and pipette, a giga-ohm seal was formed on the isolated SMVs, then currents recorded while holding the membrane at different voltages between −150mV and + 150mV. The peak conductance was 600pS on average. In some (Fig. 6a, left) but not all (Fig. 6c, left) recordings, gating between different levels of conductance was detected. Since SMVs perform ATP hydrolysis coupled to H^+ movement upon addition of ATP to the vesicles (see Fig. 5), and the F_1 portion of the F_1F_O ATPase faces the medium in the preparation[36], we reasoned that addition of ATP during recordings might produce a measurable current. In contrast, however, 0.5mM ATP consistently resulted in decreased membrane conductance of the SMVs by approximately 70% (Fig. 6a,c middle, mean data shown in second bar in Fig. 6b,d). The decrease in conductance most likely represents closure of channels and an increase in resistance caused by the effects of ATP on the membrane in series with the patched membrane.

The ATP effect suggests an ATP-responsive leak conductance associated with the F_1F_O ATPase. To determine if the change in leak conductance occured during ATP synthesis, succinate and ADP were added to mimic the conditions present during ATP synthesis. The decrease in membrane conductance was similar to that with ATP (N=3, conductance decreased by 79± 8%, p < 0.02, paired t test), suggesting that the leak conductance was equally sensitive to ADP or ATP.

To assess the role of Bcl-x_L in determining mitochondrial membrane leak conductance, Bcl-x_L was inhibited pharmacologically. Both ABT-737 and Obatoclax increased the conductance in the SMV membranes when added in the presence of ATP (Fig. 6a-d), although the leak was not affected by addition of control buffer (0.1% DMSO, Fig. S6a) or addition of ABT-737 or Obatoclax in the absence of ATP (Fig. 6b,d), indicating that the inhibitors themselves do not cause a leak.

To confirm the results obtained with pharmacological inhibition, knockdown of Bcl-x_L using shRNA lentiviruses was performed on cultured hippocampal neurons. Knockdown of Bcl-x_L was confirmed with immunoblots (Fig. 6e). Similar to non-transduced controls, SMV patch recordings made from scrambled shRNA-expressing cultures responded to ATP

application with approximately 80% decrease in peak conductance (measured from 0pA; Fig. 6f,g), while conductances from SMVs of Bcl-x_L shRNA transduced cultures had approximately 50% reduction (Fig. 6g,h). This suggests that endogenous Bcl-x_L is required for full leak closure upon ATP binding. Further studies showed that the Bcl-x_L-regulated leak conductance in SMVs is different from the oligomycin-sensitive H^+ conductance and is pharmacologically distinct from that of the ANT or K_{ATP} (Fig. S6b-g). A non-selective proteinaceous pore that shunts H^+ ions away from H^+ translocating activities found within the membrane portion of the F_1F_O ATPase protein complex is a reasonable candidate for the ATP and Bcl-x_L-regulated leak conductance.

Bax and Bak-independent cell survival depends on Bcl-x_L-regulated metabolic changes

The anti-apoptotic function of Bcl-x_L can exist independently of interaction with pro-apoptotic Bcl2 family members such as Bax and Bak[42], but the mechanism of such protection is not fully understood. Glucose-free, galactose-containing media force mitochondrial metabolism. To address if the metabolic function and the Bax and Bak independent survival function of Bcl-x_L overlapped, we studied the effects on ATP levels and cell survival of over-expression of Bcl-x_L in Bax, Bak double knockout (DKO) mouse embryonic fibroblasts (MEFs). ATP levels increased over time in Bcl-x_L expressing cells on galactose medium (Fig. S7a). The change in medium decreased survival of the MEFs; Bcl-x_L over-expression enhanced survival suggesting that increased mitochondrial ATP production by Bcl-x_L may rescue cells from metabolic compromise in the absence of Bax or Bak (Fig. S7b).

DISCUSSION

Previous studies show that Bcl-x_L increases mitochondrial biomass[9, 10]. Therefore, it was surprising to find that resting neurons expressing Bcl-x_L use less oxygen but have higher ATP levels and reduced glycolysis. Stimulated Bcl-x_L-expressing neurons use more of the total oxygen uptake for ATP production than stimulated controls. Additionally Bcl-x_L acutely increases ATP production during neuronal stimulation, because ABT-737 completely prevents such increase. These findings suggest that neuronal activity induces Bcl-x_L-dependent changes in mitochondrial metabolism. In stimulated neurons, Bcl-x_L expressed on endoplasmic reticulum (ER) membranes might influence the directed release of ER calcium toward mitochondrial calcium uptake mechanisms that could further enhance ATP synthesis[43].

Our evidence supports a Bcl-x_L and ATP-modulated H^+ leak in the inner mitochondrial membrane that reduces efficiency. 1) An ATP-sensitive leak of H^+ measured with the H^+ indicator ACMA is re-activated by pharmacological inhibitors of Bcl-x_L, 2) patch clamp recordings of SMVs reveal a large ion conductance attenuated by ATP, and reactivated by pharmacological or genetic inhibition of Bcl-x_L. The leaky membrane of control SMVs may come about by preparation of the vesicles without adenine nucleotides, but an adenine nucleotide-deficient state could also exist under pathophysiological conditions such as ischemia or neurodegenerative disorders. Reintroducing ATP or ADP rapidly closes the leak

suggesting that ATP or ADP-induced leak closure is an integral aspect of enzymatic function.

Although increased ATP synthase enzymatic activity will not in and of itself increase efficiency, recombinant Bcl-x_L protein and the Bcl-x_L inhibitors regulate enzymatic rate as measured by two assays (Fig. 4). These results raise the possibility that a change in position of certain proteins within the F_1F_O ATPase complex regulates enzymatic rate and leak closure.

Bcl-x_L has been found previously to act at the outer membrane [26–29]. How Bcl-x_L might target to the inner membrane is not known. Reports have located the related protein Bcl2 or Bcl-x_L to the inner membrane[30, 44] in the same compartment as the beta subunit of the ATP synthase[31] (and Chen and Hardwick unpublished data), and have suggested that Bax requires the F_1F_O ATPase to initiate apoptosis[45], and that oligomycin suppresses apoptosis[46]. The current study confirms and extends these findings, localizing Bcl-x_L to the beta subunit by immune-electron microscopy, by co-immunoprecipitation with the F_1F_O ATPase, and by co-immunoprecipitation with purified mammalian alpha and beta subunits. Binding of Bcl-x_L to the beta subunit is reversed by ABT-737, suggesting that the ABT-737 binding region is needed for binding to the beta subunit. In keeping with this, mutant recombinant Bcl-x_L proteins lacking the BH4 domain (N terminus) or the membrane targeting domain (C terminus) act as effectively as the full length protein to increase the rate of ATP hydrolysis.

The protein responsible for the leak channel itself is as yet unidentified. Only a few of the proteins associated F_1F_O ATPase have been characterized[37, 47]. Other ATP-sensitive candidate channels of the inner membrane include the ANT, Mito K_{ATP} and members of the UCP family[20, 48–52]. Although up-regulation of UCP activity in brain enhances neuroprotection, levels of homologues of the UCPs in healthy brain are relatively low[53–55]. It is therefore likely that we have encountered a previously undescribed conductance within the F_1F_O ATPase.

The increase in ATP production by Bcl-x_L over-expressing healthy neurons was anticipated by studies showing an increase in release of ATP and phosphocreatine in Bcl-x_L over-expressing non-neuronal cells undergoing death[7, 56]. Protection from cell death was attributed to enhanced release of ATP from mitochondria through Bcl-x_L-regulated VDAC opening in the outer membrane. Our results do not preclude Bcl-x_L activity in the outer membrane. In fact, it is likely that enhanced ATP production by the inner membrane F_1F_O ATP synthase complex requires maintaining VDAC in an open configuration to release the newly synthesized ATP into the cytosol.

Enhanced metabolic efficiency by Bcl-x_L in neurons may produce resistance to death of tumor cells[57, 58] and enhancement of cell survival shown here is independent of Bax and Bak (Fig. S7). Some tumor cells manifest metabolic changes attributed to an increase in aerobic glycolysis[59–61]. We show that healthy neurons use Bcl-x_L to produce a different kind of metabolic efficiency. Nevertheless, the changes in metabolism produced by Bcl-x_L could enhance resistance to pathological stressors including hypoxia and substrate

deprivation and could maintain cytosolic ATP levels in the face of increased energy demand provided by synaptic development, and long- or short-term changes in synaptic plasticity.

Methods

Primary cultures of rat hippocampal neurons and transfections

Primary rat hippocampal neurons were prepared as described previously[62, 63] and were transfected with 2.5 M calcium phosphate at DIV5 with an efficiency of ~1–5%. Neurons were transduced with lentiviral construct at DIV4-8 and studied at DIV10-14 with an efficiency of near 100%.

Viral constructs

Lentiviruses expressing Bcl-x_L with an N terminal GFP tag were used to transduce cultured hippocampal neurons, achieving almost 100% efficiency. Expression of GFP-Bcl-x_L facilitates determination of protein levels by Western blotting with an anti-GFP antibody (Anti-GFP Product #06-896 Upstate,1:500). Full length GFP-Bcl-x_L was subcloned into a lentiviral vector c-FUW[64]. Viral constructs were packaged in 293T cells by co-transfection with packaging plasmid delta 8.9 and envelope plasmid VSVG.48, and at 60h after transfection, virus-containing supernatant was collected and used to transduce cultured hippocampal neurons. Transduced neurons were studies at ~7 days after transduction.

Lentiviral shRNA knockdown of Bcl-x_L

The lentiviral plasmids, expressing short hairpin RNAs (shRNA) were from Open Biosystems, USA. The hairpin sequence against rat Bcl-x_L was: CGGGCTCACTCTTCAGTCGGAATAGTGAAGCCACAGATGTATTCCGACTGAAGA GTGAGCCCA For control, the scrambled, nonsilencing shRNA sequence (Open Biosystems catalog no. RHS4346) was used. Viruses were produced according to published methods[65]. The pGIPZ vector, containing either shRNA sequence against Bcl-x_L or the scrambled sequence was co-transfected with the packaging   8.9 and the vesicular stomatitis virus G protein vectors into HEK 293T cells. The supernatant was purified after 72h and added to the hippocampal cultures. The isolation of ATP F1FO ATPases was carried out 4 days after viral transduction of the neurons.

Luciferase assay for *in vitro* ATP and ADP measurements

Cellular ATP levels were measured upon acute cell membrane lysis in a plate reader (Perkin-Elmer) in the presence of Luciferin;luciferase (ApoSENSOR, Biovision, Mountain View, CA). Luminescence values were normalized to protein concentration for each well (performed by Pierce BSA method).

Cytosolic ATP-luminescence measured *in situ*

To continually monitor cytosolic ATP in intact cells, hippocampal neurons (E19) were transduced with a luciferase (firefly) lentiviral vector on DIV-4. The CSCW2-Luc-IRES-EGFP vectors were co-transfected into 293T cells with lentiviral packaging genome and envelope. Approximately 10^6 viral particles were used per 14mm coverslip containing

between 10^4–10^5 cells. Neurons were also co-transfected with plasmid DNA for either MitoGFP (control) or BCLxL-EGFP (efficiency of >50%) using magnetofection[66] (NeuroMag; OZ Biosciences)[9]. Between 4–7 days incubation, Neurobasal growth media (Invitrogen) was replaced with warm ACSF containing (in mM): NaCl (120), KCl (3.1); KH$_2$PO$_4$ (0.4); HEPES (pH 7.4; 20; NaHCO$_3$ (5); NaSO$_4$ (1.2); CaCl$_2$ (1.3); glucose (5.5) and 1mM D-luciferin (Na salt; BD BioSciences). Light output from neurons was assessed in a custom-built, heated (37°) luminometer that includes a computer-controlled UNIBLITZ high-speed electronic shutter (Vincent Associates, NY) and photo-multiplier tube (R464; Hamamatsu Photonics). 0.5mM luciferin or greater generated maximum light output for a given coverslip. Once steady state light output had been reached, mitochondrial ATP production was inhibited with oligomycin (10mg/ml). After 15min, ATP-dependent light levels were normalized for ATP by permeabilizing the neurons with a mock intracellular buffer[67]. Luciferase expression in neurons was verified by imaging single neurons for light output with a high-intensity CCD (C5405-50; Hamamatsu Photonics) mounted on an inverted microscope (Axiovert 135 TV; Carl Zeiss Inc.). A 40x oil-immersion objective with high numerical aperture (Fluar; Carl Zeiss Inc.) was used to ensure efficient light capture. Photons were integrated using custom-built acquisition software (BioCurrents Research Center).

Oxygen flux measurements

Oxygen uptake was measured in single neurons in culture using a sensitive oxygen electrode[17]. Oxygen flux was recorded using a 2–4μm dia. electrode at 5μm from the cell that was moved with a displacement of 10μm in the X-Y axes so that the oxygen-sensing electrode was positioned repeatedly closer to and farther from the cell. The current detected at two positions results in a differential current that can be translated into oxygen flux given the known oxygen concentration in the bath and the distance of the excursion of the electrode between the two points (Fig. S1A, B)[17]. The measured current associated with oxygen flux across the neuronal membrane was lower after treatment with oligomycin (Fig. S1B). The measured current was further lowered by treatment of cells with the electron transport inhibitor antimycin A (Fig. S1B). For oxygen flux measurements performed during neuronal activity, cells were perfused with osmotically-balanced extracellular solution containing high KCl (90mM KCl, 64mM NaCl, 2mM MgCl2, 10mM glucose, 10mM HEPES, 2mM CaCl2 (pH 7.4, 300 mOsm) for one minute followed by cessation of perfusion for one minute during which peak oxygen flux was measured. Cells were again perfused with normal extracellular buffer (KCl lowered to 2.5mM) for one minute, followed by addition of oligomycin (20mg/ml) to the bath. Oxygen flux was measured after cessation of perfusion and reaching a stable value for at least 5min.

F$_1$F$_O$ ATPase vesicle preparation

Rodent whole brain without cerebellum was minced in isolation buffer (IB (250mM sucrose, 20mM Hepes, pH 7.2, 1mM EDTA, BSA 0.5%)). Tissue was homogenized in a Dounce homogenizer, then centrifuged at low speed (1300rcf-set tabletop to 4000) to pellet nuclear material. Supernatant was centrifuged at high speed (13,000rcf) to pellet mitochondria and synaptosomes. Synaptosomes were disrupted with a nitrogen decompression chamber (Parr Instruments, Moline, Illinois) at 1,200psi for 10min, followed by rapid decompression.

Mitochondrial and burst synaptosomes were layered onto ficoll gradients (10% and 7.5% ficoll) and centrifuged in Beckman ultracentrifuge at 32,500rpm for 20min. Pellet was washed and resuspended in IB (approx. 4–10mg/mL protein), combined with an equal volume of digitonin (Dig 1% = 10mg/mL isobuffer), incubated on ice for 15min and centrifuged twice at 9000×g for 10min. Pellet was resuspended in 200μL of IB, and 2μL of 10% Lubrol PX (C12E9)(Calbiochem, San Diego, CA) was added, mixed, and allowed to sit on ice for 15min. Lubrol-mitochondria mixture was layered onto IB and centrifuged at 39,000rpm for 1hr. Final pellet was washed in IB and centrifugated at 13,000rpm.

Luciferase assay on F_1F_O ATPase

ATP hydrolysis was measured using the BioVision Aposensor ATP Assay Kit, according to manufacturer's protocol in presence of 30–40μg F_1F_O ATPase, and 0.5mM ATP. In some experiments, 10μL Bcl-x_L .045–0.79mg/ml, 5μg/ml Oligomycin, 1μM FCCP, nystatin (450mg/ml), 17μM ABT-737, or 0.1% DMSO were added to the mixture. Data are displayed as mM ATP hydrolysis/min/mg SMV protein. All experiments used 3 wells for each condition, and the experiments were repeated at least three times for each condition on samples from different F_1F_O ATPase isolations.

ATP synthase enzyme activity assay

The ATPase activity was measured using the assay kit from Mitosciences, USA (Catalog # MS541), according to the manufacturer's protocol and published methods[68]. Briefly, 5mg F_1F_O ATPase (per well) was detergent-extracted and immunocaptured overnight within the 96 well plates. Inhibitors of Bcl-x_L were added to the immobilized enzyme and incubated for 20min. prior to addition of the reagent mix and measurement. The oxidation of NADH to NAD+ results from a coupled reaction catalyzed by pyruvate kinase and lactate dehydrogenase in presence of phosphoenolpyruvate, dependent on ADP production by the ATPase in the presence of ATP. The change in fluorescence as NADH is oxidized was measured as a decrease in absorbance at 340nm using a PerkinElmer VICTOR3 Multilabel Plate Reader.

Electrophysiology

F_1F_O ATPase vesicle recordings were made by forming a giga-ohm seal onto F_1F_O ATPase vesicles in intracellular solution (in mM: 120 KCl, 8 NaCl, 0.5 EGTA, 10 HEPES, pH 7.3) using an Axopatch 200B amplifier (Axon Instruments) at room temperature (22–25°C). Recording electrodes were pulled from borosilicate glass capillaries (WPI) with a final resistance in the range of 80–120 MW. SMVs were visualized by phase-contrast microscopy with a Nikon or Zeiss inverted microscope. Signals were filtered at 5 kHz using the amplifier circuitry. Data were analyzed using pClamp 10.0 software (Axon Instruments). All population data were expressed as mean ± SEM. Membrane currents under different experimental conditions were assessed by measuring peak membrane current (in pA) – the baseline current. The baseline current was defined as a non-specific electrode leak current. All current measurements were adjusted for the holding voltage assuming a linear current-voltage relationship: The resulting conductances are expressed in pS according to the equation G = V/DI where G is conductance in pS, V=membrane holding voltage in mV, DI

= peak membrane current in pA - baseline current. Group data were quantified in terms of conductance.

ATP-driven quenching of 9-Amino-6-chloro-2-methoxyacridine (ACMA)

ACMA fluorescence quenching was measured according to previously published methods[69]. 2μM ACMA (Sigma-Aldrich, USA) was added to 5μg isolated F_1F_O ATPase vesicles[47], in presence of ATP (1mM), inhibitors of Bcl-x_L, Oligomycin or FCCP at concentrations described in the text (total volume of 100μl). F_1F_O ATPase vesicle suspensions were excited at 410nm, and emission was measured at 490nm, using a PerkinElmer VICTOR3 Multilabel Plate Reader.

Electron microscopy

Hippocampal neuron cultures (DIV13-14) prepared from E18 embryonic rats were transduced with lentiviruses expressing GFP or GFP-Bcl-x_L fusion protein to achieve gene expression in approximately 100% of the neurons[9], and at 7 days post infection, cultures were prepared for electron microscopy as previously described[9].

Immuno-electron microscopy

Samples (either cultured cells or whole brain) were fixed in 4% paraformaldehyde in 0.25M Hepes for 1 hour. Cultured cells were scraped and re-suspended in 10% gelatin. Samples were rinsed in PBS, chilled and trimmed to smaller blocks then placed in 2.3M sucrose overnight on a rotor at 4°C. Brain tissue was cut into small pieces and placed in 2.3M sucrose overnight on a rotor at 4°C. Samples were then transferred to aluminum pins and frozen rapidly in liquid nitrogen. The frozen block was trimmed on a Leica Cryo-EMUC6 UltraCut and 65–75nm thick sections were collected using the Tokoyasu method[70]. The frozen sections were collected on a drop of sucrose, thawed and placed on a nickel formvar/carbon coated grid and floated in a dish of PBS ready for immunolabeling. Grids were placed section side down on drops of 0.1 M ammonium chloride for 10min to quench untreated aldehyde groups, then blocked on 1% fish skin gelatin in PBS for 20mins. Single labeled grids were incubated on either a primary antibody rabbit anti-Bcl-x (Biocarta) 1:50, or mouse anti-Sod2 (Abnova) 1:150 dilutions for 30mins. A rabbit anti mouse bridging antibody (Jackson) was used for the mouse primaries before rinsing and using 10nm protein-A gold (UtrectUMC) for 30mins. Double labeled grids used the primary rabbit anti-Bcl-x and 10nm protein-A gold followed by the mouse anti-Sod;rabbit anti-mouse bridge and the 5nm protein-A gold. All grids were rinsed in PBS, fixed using 1% gluteraldehyde for 5mins, rinsed and transferred to a UA;methylcellulose drop for 10mins. Samples were viewed with a FEI Tencai Biotwin TEM at 80Kv. Images were taken using Morada CCD and iTEM (Olympus) software.

Immunoprecipitation and Western blot analysis

Cell lysate was incubated with 2μg rabbit anti anti- Bcl-x_L (54H6, Cell Signaling) and mouse anti-beta-subunit (Mitosciences) antibodies in RIPA buffer overnight at 4oC with gentle rocking. Protein G sepharose beads (Sigma-Aldrich) were added and incubated overnight at 4oC. Following (3X) washing with the lysis buffer, the bound proteins were

eluted from the beads with 2X Laemmli sample buffer. The immunoprecipitated samples were analyzed by Western blotting. For the Bcl-x_L-synthase interaction study, the human ORF constructs for alpha, beta, b, c, delta, d, epsilon, gamma and OSCP ATP-synthase subunits, tagged with Myc and DDK (Flag), from Origene Technologies (Rockville, MD), were expressed in 293T cells and purified, using the EZview^™ Red ANTI-FLAG^® M2 Affinity Gel (Sigma, USA), according to the manufacturer's protocol. The expression was verified and the binding of Bcl-x_L to individual subunits was assessed by immunoblot analysis, using the mouse anti-Myc and Rabbit anti-Bcl-x_L antibodies (Cell signaling Technology), respectively.

Western blotting for mitochondrial protein was carried out using the following antibodies: rabbit anti-human Bcl-x_L (A.G.Scientific, 1:1000), anti-GFP antibody (ab290, Abcam, 1:1000), rabbit anti-Drp1 (sc-32898, Santa Cruz, 1:1000), rabbit anti-VDAC (#4866, Cell Signaling, 1:1000), mouse anti-GAPDH, (sc-32233, Santa Cruz, 1:1000),rabbit anti-ANT (sc-11433, Santa Cruz, 1:1000), rabbit anti-PGC1alpha, (#2178, Cell signaling, 1:1000), mouse anti-COXIV, (ab14744, abcam, 1:1000).

Lactate measurements

Lactate was measured by enzyme-controlled fluorometric assay for NADPH-NADP conversion, after the method of Lowry and Passoneau (1972), using a CMA600 analyser (CMA;Microdialysis, Solna, Sweden).

Statistical analysis

For comparisons involving 2 groups, paired or unpaired Student's t-tests (2-tailed) were used. In all figures, *=$p<0.05$, **=$p<0.01$, and ***=$p<0.001$ to denote significance level, and exact p values are provided in the figure legends.

Supplementary Material

Refer to Web version on PubMed Central for supplementary material.

Acknowledgments

References

1. Banasiak KJ, Xia Y, Haddad GG. Mechanisms underlying hypoxia-induced neuronal apoptosis. Progress in Neurobiology. 2000; 62:215–249. [PubMed: 10840148]

2. Youle RJ, Strasser A. The BCL-2 protein family: opposing activities that mediate cell death. Nat Rev Mol Cell Biol. 2008; 9:47–59. [PubMed: 18097445]

3. Fannjiang Y, et al. BAK alters neuronal excitability and can switch from anti- to pro-death function during postnatal development. Developmental Cell. 2003; 4:575–585. [PubMed: 12689595]

4. Kim H, et al. Hierarchical regulation of mitochondrion-dependent apoptosis by BCL-2 subfamilies. [see comment]. Nature Cell Biology. 2006; 8:1348–1358. [PubMed: 17115033]

5. Wang C, Youle RJ. The role of mitochondria in apoptosis*. Annu Rev Genet. 2009; 43:95–118. [PubMed: 19659442]

6. Hardwick JM, Youle RJ. SnapShot: BCL-2 proteins. Cell. 138:404. [PubMed: 19632186]

7. Gottlieb E, Armour SM, Thompson CB. Mitochondrial respiratory control is lost during growth factor deprivation. Proceedings of the National Academy of Sciences of the United States of America. 2002; 99:12801–12806. [PubMed: 12228733]

8. Krajewska M, et al. Dynamics of expression of apoptosis-regulatory proteins Bid, Bcl-2, Bcl-X, Bax and Bak during development of murine nervous system. Cell Death & Differentiation. 2002; 9:145–157. [PubMed: 11840165]

9. Li H, et al. Bcl-xL induces Drp1-dependent synapse formation in cultured hippocampal neurons. Proceedings of the National Academy of Sciences of the United States of America. 2008; 105:2169–2174. [PubMed: 18250306]

10. Berman SB, et al. Bcl-x L increases mitochondrial fission, fusion, and biomass in neurons. J Cell Biol. 2009; 184:707–719. [PubMed: 19255249]

11. Mozhayeva MG, Sara Y, Liu X, Kavalali ET. Development of vesicle pools during maturation of hippocampal synapses. Journal of Neuroscience. 2002; 22:654–665. [PubMed: 11826095]

12. Verstreken P, et al. Synaptic mitochondria are critical for mobilization of reserve pool vesicles at Drosophila neuromuscular junctions. Neuron. 2005; 47:365–378. [PubMed: 16055061]

13. Li Z, Okamoto K, Hayashi Y, Sheng M. The importance of dendritic mitochondria in the morphogenesis and plasticity of spines and synapses.[see comment]. Cell. 2004; 119:873–887. [PubMed: 15607982]

14. Hickman JA, Hardwick JM, Kaczmarek LK, Jonas EA. Bcl-xL inhibitor ABT-737 reveals a dual role for Bcl-xL in synaptic transmission. J Neurophysiol. 2008; 99:1515–1522. [PubMed: 18160428]

15. Manfredi G, Yang L, Gajewski CD, Mattiazzi M. Measurements of ATP in mammalian cells. Methods (Duluth). 2002; 26:317–326.

16. Oltersdorf T, et al. An inhibitor of Bcl-2 family proteins induces regression of solid tumours. Nature. 2005; 435:677–681. [PubMed: 15902208]

17. Land SC, Porterfield DM, Sanger RH, Smith PJ. The self-referencing oxygen-selective microelectrode: detection of transmembrane oxygen flux from single cells. Journal of Experimental Biology. 1999; 202:211–218. [PubMed: 9851909]

18. Brand MD. The efficiency and plasticity of mitochondrial energy transduction. Biochem Soc Trans. 2005; 33:897–904. [PubMed: 16246006]

19. Harper ME, Bevilacqua L, Hagopian K, Weindruch R, Ramsey JJ. Ageing, oxidative stress, and mitochondrial uncoupling. Acta Physiol Scand. 2004; 182:321–331. [PubMed: 15569093]

20. Andrews ZB, Diano S, Horvath TL. Mitochondrial uncoupling proteins in the CNS: in support of function and survival. Nature Reviews Neuroscience. 2005; 6:829–840. [PubMed: 16224498]

21. Kunjilwar KK, Fishman HM, Englot DJ, O'Neil RG, Walters ET. Long-lasting hyperexcitability induced by depolarization in the absence of detectable Ca2+ signals. J Neurophysiol. 2009; 101:1351–1360. [PubMed: 19144743]

22. Bouvier D, et al. EphA4 is localized in clathrin-coated and synaptic vesicles in adult mouse brain. J Neurochem. 113:153–165. [PubMed: 20067584]

23. Rolfe DF, Brown GC. Cellular energy utilization and molecular origin of standard metabolic rate in mammals. Physiol Rev. 1997; 77:731–758. [PubMed: 9234964]

24. Hackenbrock CR, Rehn TG, Weinbach EC, Lemasters JJ. Oxidative phosphorylation and ultrastructural transformation in mitochondria in the intact ascites tumor cell. J Cell Biol. 1971; 51:123–137. [PubMed: 5111873]

25. Vander Heiden MG, et al. Bcl-xL promotes the open configuration of the voltage-dependent anion channel and metabolite passage through the outer mitochondrial membrane. Journal of Biological Chemistry. 2001; 276:19414–19419. [PubMed: 11259441]

26. Lovell JF, et al. Membrane binding by tBid initiates an ordered series of events culminating in membrane permeabilization by Bax.[see comment]. Cell. 2008; 135:1074–1084. [PubMed: 19062087]

27. Galonek HL, Hardwick JM. Upgrading the BCL-2 network.[comment]. Nature Cell Biology. 2006; 8:1317–1319. [PubMed: 17139279]

28. Boise LH, et al. bcl-x, a bcl-2-related gene that functions as a dominant regulator of apoptotic cell death. Cell. 1993; 74:597–608. [PubMed: 8358789]

29. Kaufmann T, et al. Characterization of the signal that directs Bcl-x(L), but not Bcl-2, to the mitochondrial outer membrane. J Cell Biol. 2003; 160:53–64. [PubMed: 12515824]

30. Hockenbery D, Nunez G, Milliman C, Schreiber RD, Korsmeyer SJ. Bcl-2 is an inner mitochondrial membrane protein that blocks programmed cell death. Nature. 1990; 348:334–336. [PubMed: 2250705]

31. Gotow T, et al. Selective localization of Bcl-2 to the inner mitochondrial and smooth endoplasmic reticulum membranes in mammalian cells. Cell Death & Differentiation. 2000; 7:666–674. [PubMed: 10889511]

32. Kobayashi T, et al. Ultrastructural localization of superoxide dismutase in human skin. Acta Derm Venereol. 1993; 73:41–45. [PubMed: 8095750]

33. Suzuki K, et al. Manganese-superoxide dismutase in endothelial cells: localization and mechanism of induction. Am J Physiol. 1993; 265:H1173–1178. [PubMed: 8238402]

34. Akai F, et al. Immunocytochemical localization of manganese superoxide dismutase (Mn-SOD) in the hippocampus of the rat. Neurosci Lett. 1990; 115:19–23. [PubMed: 2216054]

35. Belzacq AS, et al. Bcl-2 and Bax modulate adenine nucleotide translocase activity. Cancer Research. 2003; 63:541–546. [PubMed: 12543814]

36. Chan TL, Greenawalt JW, Pedersen PL. Biochemical and ultrastructural properties of a mitochondrial inner membrane fraction deficient in outer membrane and matrix activities. J Cell Biol. 1970; 45:291–305. [PubMed: 4254678]

37. Ko YH, Delannoy M, Hullihen J, Chiu W, Pedersen PL. Mitochondrial ATP synthasome. Cristae-enriched membranes and a multiwell detergent screening assay yield dispersed single complexes containing the ATP synthase and carriers for Pi and ADP/ATP. Journal of Biological Chemistry. 2003; 278:12305–12309. [PubMed: 12560333]

38. Nguyen M, et al. Small molecule obatoclax (GX15–070) antagonizes MCL-1 and overcomes MCL-1-mediated resistance to apoptosis. Proceedings of the National Academy of Sciences of the United States of America. 2007; 104:19512–19517. [PubMed: 18040043]

39. Caviston TL, Ketchum CJ, Sorgen PL, Nakamoto RK, Cain BD. Identification of an uncoupling mutation affecting the b subunit of F1F0 ATP synthase in Escherichia coli. FEBS Lett. 1998; 429:201–206. [PubMed: 9650590]

40. Bonanni L, et al. Zinc-dependent multi-conductance channel activity in mitochondria isolated from ischemic brain. Journal of Neuroscience. 2006; 26:6851–6862. [PubMed: 16793892]

41. Jonas EA, Buchanan J, Kaczmarek LK. Prolonged activation of mitochondrial conductances during synaptic transmission. Science. 1999; 286:1347–1350. [PubMed: 10558987]

42. Cheng EH, Levine B, Boise LH, Thompson CB, Hardwick JM. Bax-independent inhibition of apoptosis by Bcl-XL. Nature. 1996; 379:554–556. [PubMed: 8596636]

43. Rizzuto R, et al. Ca(2+) transfer from the ER to mitochondria: when, how and why. Biochim Biophys Acta. 2009; 1787:1342–1351. [PubMed: 19341702]

44. Kluck RM, Bossy-Wetzel E, Green DR, Newmeyer DD. The release of cytochrome c from mitochondria: a primary site for Bcl-2 regulation of apoptosis.[see comment]. Science. 1997; 275:1132–1136. [PubMed: 9027315]

45. Matsuyama S, Xu Q, Velours J, Reed JC. The Mitochondrial F0F1-ATPase proton pump is required for function of the proapoptotic protein Bax in yeast and mammalian cells. Mol Cell. 1998; 1:327–336. [PubMed: 9660917]

46. Shchepina LA, et al. Oligomycin, inhibitor of the F0 part of H+-ATP-synthase, suppresses the TNF-induced apoptosis. Oncogene. 2002; 21:8149–8157. [PubMed: 12444550]

47. Chen C, et al. Mitochondrial ATP synthasome: three-dimensional structure by electron microscopy of the ATP synthase in complex formation with carriers for Pi and ADP/ATP. Journal of Biological Chemistry. 2004; 279:31761–31768. [PubMed: 15166242]

48. O'Rourke B. Evidence for mitochondrial K+ channels and their role in cardioprotection. Circulation Research. 2004; 94:420–432. [PubMed: 15001541]

49. Crompton M. The mitochondrial permeability transition pore and its role in cell death. Biochemical Journal. 1999; 341:233–249. [PubMed: 10393078]

50. Costa AD, Garlid KD. MitoKATP activity in healthy and ischemic hearts. J Bioenerg Biomembr. 2009; 41:123–126. [PubMed: 19353252]

51. Liu T, O'Rourke B. Regulation of mitochondrial Ca2+ and its effects on energetics and redox balance in normal and failing heart. J Bioenerg Biomembr. 2009; 41:127–132. [PubMed: 19390955]

52. Porter RK. Uncoupling protein 1: a short-circuit in the chemiosmotic process. J Bioenerg Biomembr. 2008; 40:457–461. [PubMed: 18958609]

53. Diano S, et al. Uncoupling protein 2 prevents neuronal death including that occurring during seizures: a mechanism for preconditioning. Endocrinology. 2003; 144:5014–5021. [PubMed: 12960023]

54. Horvath TL, Diano S, Barnstable C. Mitochondrial uncoupling protein 2 in the central nervous system: neuromodulator and neuroprotector. Biochem Pharmacol. 2003; 65:1917–1921. [PubMed: 12787871]

55. Sullivan PG, Springer JE, Hall ED, Scheff SW. Mitochondrial uncoupling as a therapeutic target following neuronal injury. J Bioenerg Biomembr. 2004; 36:353–356. [PubMed: 15377871]

56. Vander Heiden MG, et al. Outer mitochondrial membrane permeability can regulate coupled respiration and cell survival. Proceedings of the National Academy of Sciences of the United States of America. 2000; 97:4666–4671. [PubMed: 10781072]

57. Chonghaile TN, Letai A. Mimicking the BH3 domain to kill cancer cells. Oncogene. 2008; 27 (Suppl 1):S149–157. [PubMed: 19641500]

58. Vander Heiden MG, Cantley LC, Thompson CB. Understanding the Warburg effect: the metabolic requirements of cell proliferation. Science. 2009; 324:1029–1033. [PubMed: 19460998]

59. Frezza C, Gottlieb E. Mitochondria in cancer: not just innocent bystanders. Semin Cancer Biol. 2009; 19:4–11. [PubMed: 19101633]

60. Warburg O. On respiratory impairment in cancer cells. Science. 1956; 124:269–270. [PubMed: 13351639]

61. Golshani-Hebroni SG, Bessman SP. Hexokinase binding to mitochondria: a basis for proliferative energy metabolism. J Bioenerg Biomembr. 1997; 29:331–338. [PubMed: 9387093]

62. Krueger SR, Kolar A, Fitzsimonds RM. The presynaptic release apparatus is functional in the absence of dendritic contact and highly mobile within isolated axons. Neuron. 2003; 40:945–957. [PubMed: 14659093]

63. Brewer GJ. Isolation and culture of adult rat hippocampal neurons. Journal of Neuroscience Methods. 1997; 71:143–155. [PubMed: 9128149]

64. Lois C, Hong EJ, Pease S, Brown EJ, Baltimore D. Germline transmission and tissue-specific expression of transgenes delivered by lentiviral vectors. Science. 2002; 295:868–872. [PubMed: 11786607]

65. Komai S, et al. Postsynaptic excitability is necessary for strengthening of cortical sensory responses during experience-dependent development. Nat Neurosci. 2006; 9:1125–1133. [PubMed: 16921372]

66. Buerli T, et al. Efficient transfection of DNA or shRNA vectors into neurons using magnetofection. Nat protoc. 2007; 2:3090–3101. [PubMed: 18079708]

67. Gajewski CD, Yang L, Schon EA, Manfredi G. New insights into the bioenergetics of mitochondrial disorders using intracellular ATP reporters. Mol Biol Cell. 2003; 14:3628–3635. [PubMed: 12972552]

68. Lotscher HR, deJong C, Capaldi RA. Inhibition of the adenosinetriphosphatase activity of Escherichia coli F1 by the water-soluble carbodiimide 1-ethyl-3-[3-(dimethylamino)propyl]carbodiimide is due to modification of several carboxyls in the beta subunit. Biochemistry. 1984; 23:4134–4140. [PubMed: 6237683]

69. Nieuwenhuis FJ, Kanner BI, Gutnick DL, Postma PW, van Dam K. Energy conservation in membranes of mutants of Escherichia coli defective in oxidative phosphorylation. Biochim Biophys Acta. 1973; 325:62–71. [PubMed: 4149157]

Author Manuscript Author Manuscript Author Manuscript Author Manuscript

70. Tokuyasu KT. A technique for ultracryotomy of cell suspensions and tissues. J Cell Biol. 1973; 57:551–565. [PubMed: 4121290]
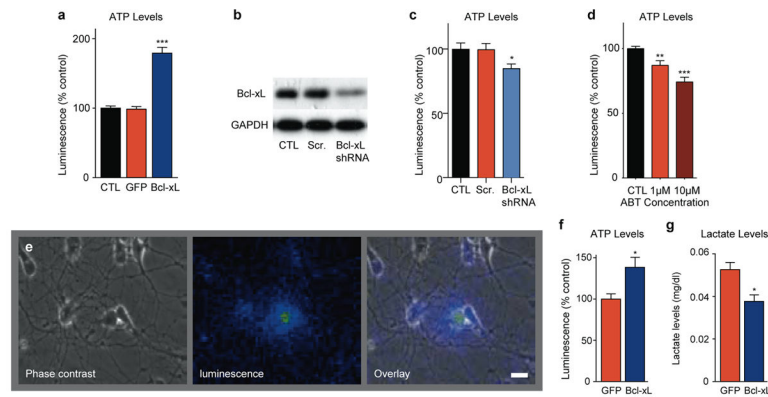
Figure 1. Cellular ATP levels are altered by Bcl-x$_L$ over-expression or depletion in hippocampal neurons

a. ATP levels as measured by firefly Luciferin;luciferase luminescence at 7 days after transduction with lentivirus constructs. Luminescence level was normalized to protein level in each individual well, N= 8 wells, ***p < 0.0001). At least three independent experiments of different cultures showed similar results.

b. Western blot for endogenous Bcl-x$_L$ protein. Cell lysates prepared from non-transduced control hippocampal neuron cultures (CTL), scrambled shRNA expressing neuron cultures and Bcl-x$_L$ shRNA expressing neuron cultures at 4 days after viral transduction. GAPDH serves as a loading control.

c. ATP levels as measured by firefly Luciferin;luciferase luminescence in control cultures or cultures expressing Bcl-x$_L$ shRNA or scrambled shRNA at 4 days after viral transduction. Luminescence level was normalized to protein level in each individual well (N=11 for each condition, representing two independent cultures; *p<0.03).

d. ATP levels as measured by firefly Luciferin;luciferase luminescence in control cultures or cultures exposed for 12–18hrs to ABT-737 at the indicated concentrations. Luminescence level was normalized to protein level in each individual well (N=15 for each condition, **p<0.004 ***p<0.0001, three independent cultures).

e. Example image of a neuron expressing CSCW2-Luciferase lentiviral vector. Light is produced in response to application of 1mM luciferin. Shown are phase, luminescent and overlay images. In pseudocolor images, blue is low luminescence, yellow is high luminescence. Scale bar: 20μm.

f. Group data for amount of ATP represented by luminescence per coverslip of living hippocampal neurons at 7 days after transfection with indicated constructs. Light levels were normalized to average of light levels in mito-GFP control cells. Living neurons were transfected with CSCW2-luciferase-IG lentivirus vector and mito-GFP or GFP-Bcl-x$_L$ (N= 8 coverslips from at least three independent cultures for mito-GFP-expressing neurons, N=10 coverslips from at least three independent cultures of GFP-Bcl-x$_L$ expressing neurons, * P < 0.02).

g. Lactate levels in medium surrounding GFP-Bcl-x$_L$ expressing neurons compared to GFP expressing controls after 12hrs in physiological (5mM) glucose medium (one culture, N=3 replicates for each condition *p< 0.02). For all panels error bars indicate SEM.
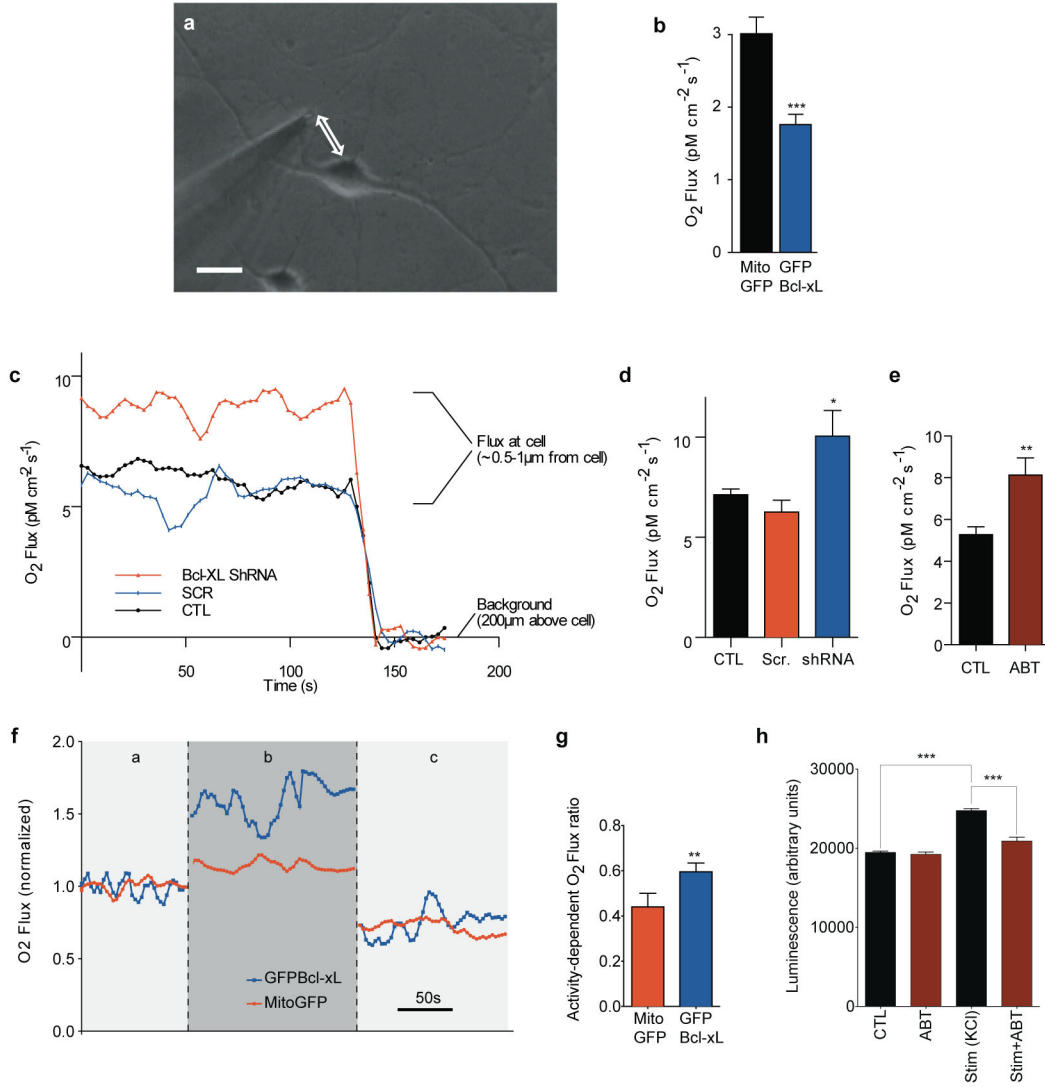
Figure 2. Bcl-x_L alters oxygen uptake by neurons. Resting Bcl-x_L over-expressing and Bcl-x_L depleted neurons have altered oxygen uptake

a. Photomicrograph of self-referencing amperometric O_2 microsensor positioned next to a single hippocampal neuron. Scale bar: 20μm.

b. Group data for basal respiration in GFP- Bcl-x_L expressing neurons compared with Mito-GFP expressing neurons at 7 days after transfection (N=28 Mito-GFP expressing neurons, N=26 GFP- Bcl-x_L expressing neurons; ***p<0.0005). Experiment was repeated in 5 different cultures from 5 different animals.

c. Representative traces of oxygen flux levels of single neurons. For neuronal flux measurements, self-referencing amperometric O_2 microsensor was placed within 1μm of the cell surface. For background measurement, electrode was moved 200μm from the cell surface.

d. Group data for basal respiration levels of single non-expressing neurons, or neurons expressing Bcl-x_L shRNA or scrambled shRNA at 7 days after viral transduction (N=10

replicates for CTL and Bcl-x_L shRNA, N=9 replicates for scrambled shRNA, at least three independent cultures were used for studies; *p<0.05).

e. Group data for basal respiration levels of single control neurons or neurons exposed for 18hrs to 10μM ABT-737 (N=26 for control and 19 for ABT-737; **p< 0.002; at least three different cultures for each group).

f. Representative traces of oxygen flux levels of single neurons expressing Bcl-x_L-GFP or mito-GFP, while resting (a), stimulated with 90mM KCl (b) and after addition of 5mg/ml oligomycin (c). All values were normalized against the average oxygen flux of the same neuron at resting flux level.

g. Group data for the oxygen flux of single cultured neurons expressing Bcl-x_L-GFP or mito-GFP. Leak-subtracted oxygen flux was divided by peak oxygen flux measured during neuronal activity [ratio = (b-c)/b]. Neurons were studied from four independent cultures (N=9 Mito-GFP control neurons, N=12 GFP-Bcl-x_L expressing neurons, *p<0.04).

h. Luminescence of firefly luciferase in cultured hippocampal neurons exposed or not to 1μM ABT-737 for 5min. and subsequently stimulated with 90mM KCl for 90s (N=12 wells per group; ***p<0.0001; two different cultures for each condition). Measurement of stimulated wells was taken 5min. after washout of high K. For all panels error bars indicate SEM.
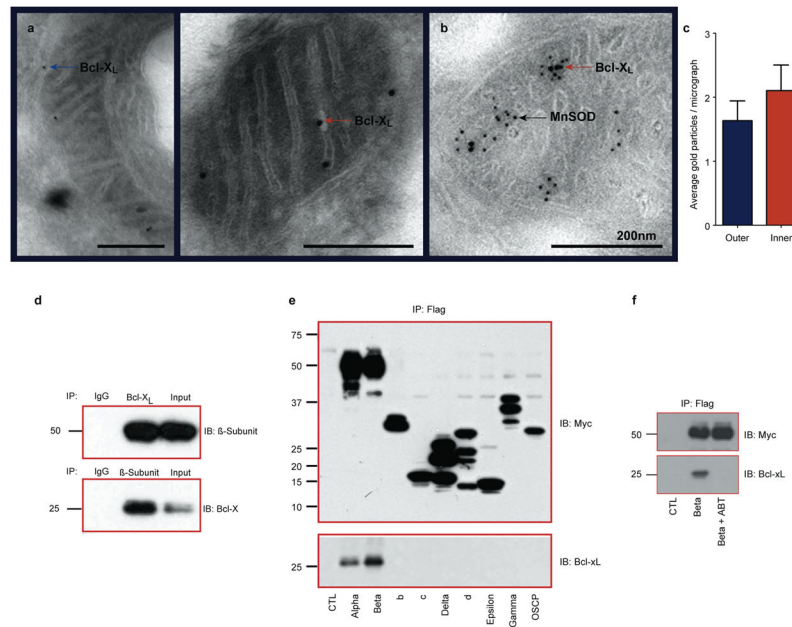
Figure 3. Bcl-x$_L$ is expressed in the mitochondrial inner membrane and interacts with ATP synthase

a. Immuno-electron micrographs from cultured neurons over-expressing Bcl-x$_L$ at 7 days after viral transduction. Bcl-x$_L$ immunoreactivity in the outer membrane (left panel, arrow) and the inner membrane cristae (right panel, arrow) are shown. Scale bars: 200nm.

b. Immuno-EM prepared from untreated rat brain (large balls: Bcl-x$_L$; small balls: MnSOD).

c. Average number of immunogold particles per electron micrograph representing Bcl-x$_L$ protein in the outer vs. inner membrane (N=30 micrographs). Error bars indicate SEM.

d. Reciprocal immunoblots of co-immunoprecipitation of Bcl-x$_L$ and ATP synthase beta-subunit from purified rat brain ATP synthase complex. Antibodies are as indicated (IB) (N=3). Top lane: the precipitating antibodies were IgG and Bcl-x$_L$. The top right lane represents the whole cell lysate. Bottom lane: the precipitating antibodies were IgG and ATP synthase beta subunit. The bottom right lane represents the whole cell lysate.

e. Immunoprecipitation of the Myc-Flag-tagged ATP synthase subunits (Alpha, Beta, b, c, Delta, D, Epsilon, Gamma, and Oscp), precipitated using the anti-Flag affinity gel and immunoblotted using anti-myc tag antibody (upper panel). (Lower panel): Western blot analysis, using anti-Bcl-x$_L$ antibody, on the immunoprecipitated samples.

f. Immunoprecipitation of the Myc-Flag-tagged ATP synthase subunit Beta, precipitated using the anti-Flag affinity gel and immunoblotted using anti-myc tag antibody (upper panel). Cells were pre-exposed for 12hr to 1μM ABT-737 or vehicle. (Lower panel): Western blot analysis, using anti-Bcl-x$_L$ antibody on the immunoprecipitated samples.
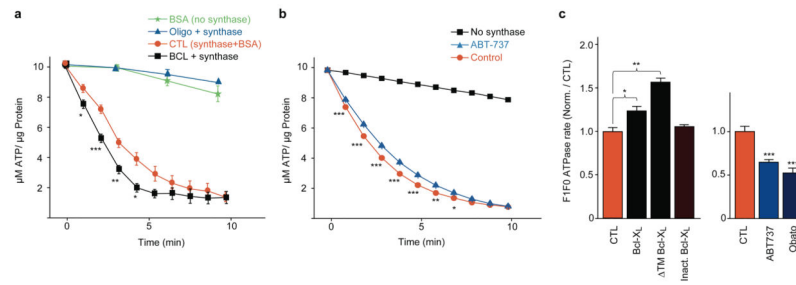
Figure 4. Bcl-x$_L$ protein regulates ATPase activity

a. Luminescence of firefly Luciferin;luciferase activity in the presence of ATP. N=3 wells without F$_1$F$_O$ ATP synthase (blank); N=3 wells F$_1$F$_O$ ATP synthase plus the F$_O$ inhibitor oligomycin (5mg/ml); N=6 wells synthase plus recombinant Bcl-x$_L$ protein (0.045–0.79mg protein/ml); N=9 wells synthase plus control protein (0.05mg/ml BSA, F$_1$F$_O$ ATP synthase concentration for all experiments was 4mg protein/ml). *p < 0.05, **p < 0.005, ***p<0.0005. Experiments on Bcl-x$_L$ vs. control were repeated and confirmed on 5 different experimental days using at least two different F$_1$F$_O$ ATPase vesicle preparations (from two different animals).

b. F$_1$F$_O$ ATPase activity of purified F$_1$F$_O$ ATP synthase in the absence and presence of ABT-737 (20μM). Data are displayed as percent change in fluorescence over time (N=3 for each condition; ***p< 0.0008, **p<0.003, *p<0.04). Experiments were repeated on three independent isolations with similar results.

c. F$_1$F$_O$ ATPase activity of the purified F$_1$F$_O$ ATP synthase vesicles in the presence of the indicated recombinant proteins or reagents as a function of the rate of decrease in NADH fluorescence (see Methods). *(Left panel)* N=3 samples in each condition, **p<0.002,*p<0.04, assay performed with similar results on two independent F$_1$F$_O$ ATP synthase isolations. *(Right panel)* N=7 samples for each condition, assay performed with similar results on two independent isolations***p<0.0001. For all panels error bars indicate SEM.
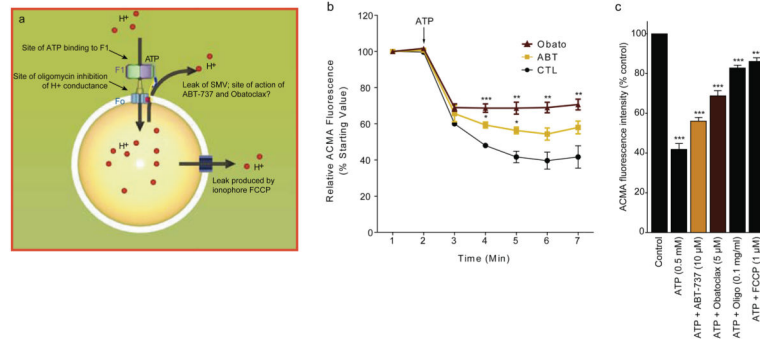
Figure 5. ATP-sensitive H^+ ion sequestration into F_1F_O ATPase vesicles (SMVs) is attenuated by Bcl-x_L inhibitors, and by oligomycin and FCCP

a. Arrangement of F_1F_O ATPase vesicle exposed to the fluorescent pH indicator, ACMA. ATP binds to F_1 to activate ATP hydrolysis and drives H^+ ions through F_O, decreasing ACMA fluorescence. Bcl-x_L inhibitors produce an H^+ leak out of the F_1F_O ATPase membrane, perhaps at the site of the F_1F_O ATPase itself, resulting in an increase in ACMA fluorescence. Oligomycin blocks movement of H^+ ions through the F_O, and thus prevents a drop in ACMA fluorescence. FCCP is an H^+ ionophore that causes the leakage of H^+ out of the SMV.

b. Example traces of fluorescence changes of ACMA indicator over time in the presence of F_1F_O ATPase vesicles (N=3 samples for each condition, repeated three times. Comparing effects of reagents in the presence of ATP to the effect of ATP alone, * $p < 0.05$; ** $p < 0.01$; ***$p < 0.0001$, one-way ANOVA).

c. Group data showing peak effect on relative fluorescence (% control). Control represents fluorescence of ACMA indicator in the presence of SMVs before the addition of ATP (N=3 samples for each group. * $p < 0.05$; ***$p<0.0001$, one-way ANOVA. This study was repeated at least three times on different batches of SMVs with similar results. Error bars indicate SEM.
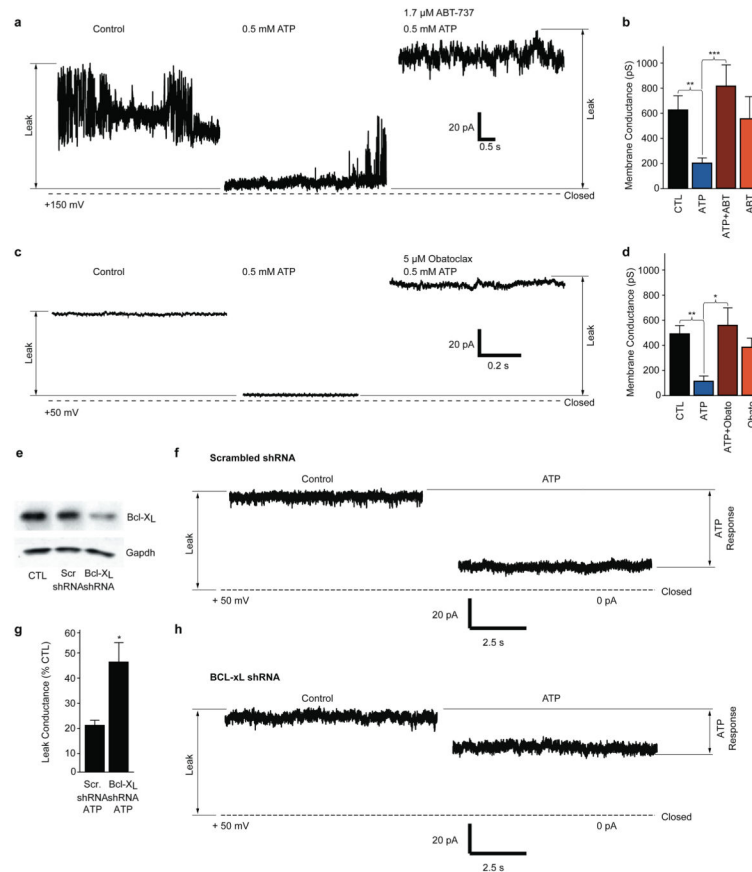
Figure 6. Pharmacological inhibition or depletion of Bcl-x$_L$ reverse leak closure in patch clamp recordings of isolated ATP F$_1$F$_O$ ATPase vesicles

a. Example SMV patch recording at the indicated voltage before and after ATP and ATP +ABT-737 exposure. Dotted line represents 0pA.

b. Group data of membrane conductances of all recordings such as shown in *a* (SMV recordings from left to right, N=30, 23, 19, 7; **p< 0.002, ***p<0.0009). The last histogram shows experiments in which the Bcl-x$_L$ inhibitor was added to patches in the absence of ATP.

c. Example SMV patch recording at the indicated voltage before and after ATP and ATP +Obatoclax exposure. Dotted line represents 0 pA.

d. Group data of membrane conductances of all recordings such as shown in *c* (SMV recordings from left to right, N=23, 9, 15, 14; **p< 0.004, *p<0.04). The last histogram shows experiments in which the Bcl-x$_L$ inhibitor was added to patches in the absence of ATP.

e. Western blot for endogenous Bcl-x$_L$ protein. Cell lysates prepared from non-transduced control hippocampal neuron cultures (CTL), scrambled shRNA expressing neuron cultures and Bcl-x$_L$ shRNA expressing neuron cultures at 4 days after transduction. Protein concentration was controlled by immunoblotting for GAPDH.

f. SMV patch recordings before and after the addition of 0.5mM ATP. SMVs were prepared from hippocampal neurons expressing control (scrambled) shRNA at 4 days after transduction.

g. Group data from all recordings of control (scrambled) shRNA or Bcl-x_L shRNA. Shown is the membrane leak conductance remaining after the addition of ATP as a percent of the initial conductance before the addition of ATP (N=5 control recordings, N=7 shRNA Bcl-x_L recordings; *p< 0.03).

h. SMV patch recordings before and after the addition of ATP. SMVs were prepared from hippocampal neurons expressing Bcl-x_L shRNA at 4 days after transduction. For all panels error bars indicate SEM.